Temperature effect on the synthesis of Iron-Cobalt Nano-particles using Catalytic Chemical Vapor Deposition of CO_2 in Thermo-gravimetric Analyzer: Analytical and Thermodynamic Studies

Muhammad F. Irfan[*,†], A. Aramaniya[*]

Present address: [†]Department of Chemical Engineering, College of Engineering, University of Bahrain, 32038, Isa Town, Kingdom of Bahrain, Phone: +97317876392, Fax: +97317680935, E-mail address: mfirfan@uob.edu.bh (M.F. Irfan-Corresponding author)

Previous address: [*]Department of Chemical Engineering, Faculty of Engineering, University of Malaya, 50603, Kuala Lumpur, Malaysia

Abstract

Iron, cobalt and Fe-Co catalysts were prepared by conventional precipitation (co-precipitation for Fe-Co) method for the synthesis of nano-particles, using CO_2 as the carbon precursor by catalytic chemical vapor deposition. Synthesis was done in a thermo gravimetric analyzer at different temperatures ranging from 450 ^oC to 1000 ^oC particularly for Fe-Co nano particles. Products were then evaluated using the FESEM, TEM, XRD and EDS analyses. Nano-particles of pebble-like shapes with some of conjoined shapes were observed at different temperatures for Fe, Co and Fe-Co. It was also observed that increase in temperature not only enhanced the size of the nanoparticles but it also led to a greater sphericity and crystallinity of the nanoparticles. For Fe-Co alloy, the dimensions of nanoparticles were found using FESEM to be 51±1 nm, 54±1 nm, 72±1 nm and 165±1 nm at 500, 600, 700, and 800°C, respectively. TEM also shows similar results to that of FESEM. XRD results show that at lower temperature (500 ^oC), products are amorphous in nature but at higher temperature (800 ^oC), the peaks became much longer and sharper indicating the crystalline nature of Fe-Co nanoparticles. CO disproportionation reaction was discussed and equations for equilibrium constant and mole fraction (y_{CO} and y_{CO_2}) were developed. It was observed that CO decomposition is thermodynamically limited from 520 to 800 ^oC which led to carbon deposition on the catalyst as observed by the carbon presence in EDS, XRD and TEM images i.e. the encapsulation of thin layer of carbon on the Fe-Co particles.

Keywords: Fe-Co nanoparticles, CCVD, TGA, CO disproportionation, Carbon deposition

1. Introduction

The study on nano-particles has become a very important field of research particularly in materials science. Metal nano-particles often show exciting electronic, magnetic, optical, and chemical properties, which depend on their size, shape, surface composition, and surface atomic arrangement [1-7]. Among all magnetic materials such as metals and their oxides, cobalt and iron are well-known for their excellent magnetism. In addition, cobalt has been found to improve the coercivity of material (higher coercivity of Fe–Co alloys) as compared to pure iron [8]. The produced alloy (Fe–Co) can be used in various engineering applications due to its good, soft magnetic properties [9]. This nano-composite material is expected to have superior magnetic properties under high frequency and temperature operation, in contrast to usual ferrite.

Due to the high vulnerable surface area of metal nano-particles, they are easily oxidized in air atmosphere. Also in biomedical applications the metallic core has to be protected from the biological environment by a biocompatible and chemically stable coating [10]. Thus, to make these metal nano-particles practically applicable, it is necessary to coat them with air-stable materials like carbon. Carbon-encapsulation provides an in-expansive way to protect the nanoparticles from oxidation [11]. Carbon-encapsulated metal nano-particles consist of composite material with a metallic core and carbon shell structure on the nano-scale. The nanostructures of these carbon-encapsulated metal nano-particles regularly reveal unique phase, size and shape, which significantly influence their physical and chemical properties [12]. Physical properties of carbon-encapsulated metal nano-particle such as the saturation magnetization and the coercivity are considerably affected by the alloy formation and the microstructure. Therefore, control over the microstructure in terms of the internal strain, crystal structure and grain size (or particle size) is required to considerably improve the magnetic properties during the fabrication of nano-structured materials [13]. Due to aforementioned

properties, it has been used widely in different array of applications such as energy conversion and storage [14-16], batteries [17,18], hyperthermia [19], bio-imaging [20], water remediation [21], oxygen reduction reaction [22], microwave absorption [23], catalysis [24-26], MRI contrast agent [27], magnetorheology and magnetic data storage [28-30] and pollutant removal [31-33].

Several physical, chemical and mechanical methods exist for the synthesis of nano-particles such as electric arc discharge [34], laser ablation [35], chemical vapour deposition (CVD) [23, 36-39], detonation [40], solvothermal [41], pyrolysis [42-44] and ultrasonication [45]. The chemical synthesis of nano-particles has rapidly grown with a great potential in the preparation of high quality nano-particles at relatively low cost because of using moderate temperature (less than 1000 ^{o}C). As CVD technique is well established, gives high yield, and has the ability to scale-up, so these additional merits make CVD method more advantageous compared to the rest of the methods [36, 39, 46-48]. In the CVD method, the flowing gas can be a carbon-rich source (e.g. C_2H_2, CH_4, C_2H_5OH, CO_2 etc.) in the presence of a metal catalyst at elevated operating temperature. Under these conditions, the gaseous carbon molecules decompose, and subsequently converted into carbon coating [49, 50]. Since Fe–Co nano-particles are used in the computer read/write heads and microelectromechanical systems as magnetic recording write head and microactutors [51, 52] and in the electronic bearings and power generators of aircraft engines [53, 54] so there is interest in the preparation of Fe–Co nanoparticles. For this purpose, in the present study, CCVD method was applied to synthesize carbon coated metallic nano-particles particularly Fe-Co alloys by varying different operating temperatures under carbon dioxide environment in TGA reactor. Carbon dioxide was selected as the carbon source due to its low price, availability and low toxicity in producing and coating of nano-particles. Firstly Fe, Co and Fe-Co metal catalysts were prepared by precipitation (co-precipitation) method and later carbon coated nanoparticles were synthesized by the reduction of CO_2 using

CVD process at different temperatures. Effect of temperature on the carbon encapsulated nanoparticle's growth, dimension and nature of Fe, Co and Fe-Co was studied under carbon dioxide environment in TGA reactor. Thermodynamic study of CO_2 reduction (the CO disproportionation (carbon deposition by CO_2 reduction)) was also the part of this work for which the equilibrium constant and mole fraction relations were developed and studied with respect to temperature. The use of inexpensive carbon precursor in a very simple and cheap setup for the synthesis of carbon coated nanoparticles at different temperatures leads to the novelty of this work. The produced nanoparticles were characterized by means of scanning and transmission electron microscopies (SEM, TEM), x-ray diffraction (XRD) as well as Energy-dispersive X-ray spectroscopy (EDS).

2. Experimental

2.1. Materials

The chemicals ($Fe(NO_3)_3 \cdot 9H_2O$, $Co(NO_3)_2 \cdot 6H_2O$ and ammonia) were all of analytical reagent grade and used without any further treatment. Carbon dioxide with high purity (99.5) was used as the carbon source. The deionized water of resistivity >18MΩ was used for making all solutions.

2.2. Catalyst preparation

The catalysts were prepared via the precipitation method with iron (Fe) and cobalt (Co) as the metallic materials. In the precipitation method, 20 g of $Fe(NO_3)_3 \cdot 9H_2O$ was dissolved in 50 ml of water and ammonia solution of 0.1 M was added into the solution at atmospheric condition until pH reading of 8 was reached. The mixture was left for 2 hours; and then filtered. The solids from the filter were dried in the oven at 110°C overnight and calcined at 450°C in the air for 3 hours. The same method was used to prepare cobalt catalyst. In the preparation of Fe–Co co-precipitation method was used. For that purpose, 20 g of each $Fe(NO_3)_3 \cdot 9H_2O$ and

$Co(NO_3)_2 \cdot 6H_2O$ were dissolved in 100 ml of water. The subsequent steps were the same as those for the preparation of both Fe and Co catalysts, with the exception that the solids obtained from the filter were dried at 90°C overnight.

2.3. Synthesis of nano-particles

For the synthesis of nano-particles, the catalyst (Fe, Co or Fe–Co) of about 84 mg was placed in a thermo gravimetric analysis (TGA/SDTA851e Ultramicro Balance of Mettler Toledo) reactor. At the beginning, the sample was heated in the presence of nitrogen to drive out the air. Then, carbon dioxide was introduced with a flow rate of 50 ml/min as temperature was increased gradually from 450 to 1000 °C to evaluate the effect of synthesis temperature on the structure of nano-particle. The heating rate was set at 10 K/min and the sample was remained at final temperature for about 2 hours. Afterwards, the system was cooled down to room temperature in nitrogen atmosphere. The mass change in catalyst was also recorded.

2.4. Characterization of nano-particles

Field Emission Scanning Electron Microscopy (FESEM) analysis was performed by means of a Auriga-39-22 FESEM with an accelerating voltage used between 1 and 10 kV equipped with an EDAM III energy dispersive X-ray (EDS) analysis unit. FESEM images were used to observe the surface morphology of particles formed at different reaction temperatures. The chemical compositions of particles were investigated by the EDS analyses. For the observation, the samples were analyzed in a vacuum system between 9.85×10^{-7} mbar and 6.59×10^{-3} mbar. High-resolution transmission electron microscopy (HRTEM) was performed using a FEI Tecnai F 30 TEM with field emission gun at 300 kV. A Miniflex X-ray diffractometer (XRD) with Cu Ka radiation was used at room temperature to identify the crystal structure. The powders were first dispersed in ethanol and inserted in ultrasonic bath for 30 min and then the suspension was dispersed drop wise onto a glassy carbon slide to make a thick film.

3. Results and discussion

3.1. Characterization studies

3.1.1. Thermo-gravimetric (TG / DTG) studies

TG and DTG profile vs reaction time and reaction temperature over Fe-Co catalyst at 500 ^{o}C is shown in figure 1. The TG profile (black line) reflects the mass loss percent vs temperature during the synthesis process of nano particles upto 500 ^{o}C. TG profile (red line) reflects the mass loss percent vs time for the whole process (isothermal and non-isothermal). As temperature increased, a steady mass loss was observed with sharp decrease in mass as temperature approached 500 °C. The sample then continued at its steady mass loss, as the temperature was fixed at 500°C until the reaction time (2 hrs) was over. At the end of reaction time, the release of volatile molecules was still taking place which shows that longer reaction time is required to determine when it will stop. In addition, there was no gain of weight observed indicating no oxidation process occurred. DTG curve (blue line) gives the idea about the mass loss variation from the sample while heating during the synthesis process [55]. The peaks of mass loss at 100 -150 ^{o}C is related to water loss, which is approximately 33.92 % with respect to overall loss of the sample. This water loss occurs in two steps, dehydration and adsorbed water molecules [26, 56]. The peaks at 300 - 400 ^{o}C reflect mass loss either due to volatile matter removal from the sample or may be due to decomposition of carbon layers as reported by Sankar et al. [57]. This percentage loss is about 15.70% with respect to the total loss of sample. At higher temperatures, the changes occur in DTG curve indicates phase and magnetic transitions [58]. These results validate the carbon coating on the Co-Fe alloy, which is expected to give significant influence on the electrochemical performance. The same trends (as reflected in figure 1) were observed for all samples related to the production of nano-particles. The results of overall mass loss in TGA of the few samples are summarized in Table 1. Data in table show that higher mass loss takes place at high temperature. Sample 5 has the

largest mass change as the reaction temperature was set the highest at 600°C; whereas sample 4 has the smallest mass change as the reaction temperature was lowest at 450°C. This table also shows that at 500 ^{o}C almost same amount of mass loss occurs at all samples used. However, the mass loss is relatively small in case of Co than the rest of the samples (Fe, Fe-Co) at the same conditions.

3.1.2. Field Emission Scanning Electron Microscopic studies

Figures 2-4 are the FESEM images of the nano-particles produced under the synthesis conditions at different temperatures. All images indicate the formation of nano structured material after introducing carbon dioxide on the three catalysts (Co, Fe, Fe-Co). The images show homogeneous, packed distribution of the nano-particles and this was well established that all the three catalysts were active in the formation of carbon nano-particles, and the morphologies exhibit pebble-like shapes, with some of conjoined shapes. Figure 2 is the FESEM image of nano-particles on Co catalyst with average dimensions of 93±1 nm. This shows almost all cobalt particles are homogeneous in shape and size and they have flaky surface. However, there are very few particles of smaller dimension (47±1 nm) and a very few of bigger dimensions (132±1 nm). In other words, these particles are in the range from 47±1 to 132±1 nm. Since the particles are uniformly distributed, the cobalt surface has homogeneous properties. It is also visible in figure 2 that increase in final temperature causes an increase in nanoparticle sizes and change in their shapes. At the final temperature of 450 ^{o}C (Figure 2a), as mentioned earlier the average particle size is about 93±1 nm. However, by increasing the final temperature to 500 °C, more homogeneity in the size and shape of nano-particles are found in the produced samples. Growth of the smaller particles cause decrease in free spaces between the nano-particles. Furthermore, shape of these nano-particles becomes more spherical. Increasing the temperature to more than 500 °C (average particle size of 107±1 nm i.e. Fig 2b) causes an increase in nano-particle size as well as particle size distribution.

Adherence of the growing particles is visible in the final temperatures over 500 °C, which makes an almost even surface of nano-particles without any space between them at temperature of 650 °C (Fig. 2d) with an average particle size of 190±1 nm. This increase in size of nanoparticles with the increase of temperature indicates the dominancy of the growth stage over the nucleation stage as these two stages (nucleation and growth stages) are involved in metal nano-particle formation. In other words, smaller particles are obtained when the nucleation stage becomes predominant during the synthesis of the particle. On the other hand, when the growth process becomes dominant, bigger particles are obtained. Figure 3(a) shows nanoparticle on Fe catalyst nano particles with average dimensions of 44±1 nm. The Fe particles are smaller in size with non-uniform size and distribution. In addition, they are also irregular in shape. Hence, this gives much more heterogeneous surface properties. However, size of these nano-particles are about half of cobalt ones. Similar to cobalt, increase in final temperature causes an increase in size of growing nano-particles and therefore decreases in spaces between them. At 450 ^{o}C, the average nanoparticle was found to be 44±1 nm (Fig. 3a), however, at 500 ^{o}C (Fig. 3b), 600 ^{o}C (Fig. 3c) and 650 ^{o}C (Fig. 3d), the average particles were found to be 49±1 nm, 54±1 nm and 67±1 nm, respectively. Shape of the produced nano-particles at temperature of 600 °C is also spherical than the other iron samples. This sample also shows narrower particle size distribution in its surface than the other samples.

Figures 4 shows the nano-particles produced using Fe-Co catalysts at wide range of temperatures ranging from 450°C to 1000 ^{o}C. When the temperature was increased, the pebble-like structure showed greater sphericity and increased in sizes [59]. Heating the produced samples under flow of CO_2 until 450 °C (Fig. 4a) did not produce well-developed nano-particles, which shows that the final temperature was not sufficient for the nano-particles to be developed notably. However, as can be seen in Fig. 4b, increasing the temperature to 500 °C, increases density of nano-particles on the surface of metal and their growth increases. Effect

of temperature on nano-particles of Fe-Co can be seen in Fig. 4 (b, c, d, and f) for the final temperatures of 500 °C to 800 °C is similar to that of iron and cobalt samples. However, the size of the produced nano-particles in Fe-Co samples are between those of iron and cobalt samples i.e. 51±1 nm at 500 ^{o}C, 55±1 nm at 600 ^{o}C, 72±1 nm at 700 ^{o}C and 165±1 nm at 800 ^{o}C. It shows that on the Fe-Co catalyst, the reaction temperature played an important role in the synthesis process, as the size of nano-particles increases when temperature is increased. From figure 4g of FESEM, it can also be seen that at very high temperature i.e. 1000 ^{o}C, not only increased the size of the particles but also converted spherical particles into platelets of average size of 682±1 nm. Additionally, it seems that platelets are in layer and diffused into one another with no space between them as shown in Fig 4g and Fig 4g1. This may be due to the partial sintering of the formed metallic phase at higher temperature compared to lower temperature where the surface facilitates the diffusion of CO_2 [59]. In terms of particle sizes, it can also be said that addition of Fe in Co (Fe-Co) shows the dominant effect of Fe on Co as the size of the produced nano particle are close to the Fe particle sizes. e.g. at 500 ^{o}C and 600 ^{o}C, the average size of Fe nanoparticles are 49±1 nm and 54±1 nm and for the Fe-Co catalyst the average size of nanoparticles are almost the same i.e. 51±1 nm and 55±1 nm respectively. This clearly shows the dominancy of the Fe on Co nanoparticles during the synthesis process.

3.1.3. XRD, EDS and HRTEM studies

Diffraction peaks of XRD data correspond only to the Fe-Co alloy at two different temperatures i.e. 500 ^{o}C and 800 ^{o}C are recorded and presented in figure 5. These temperatures are selected based on the CO disproportionation reaction which is kinetically and thermodynamically limited from 520 ^{o}C to 800 ^{o}C. From XRD, it was observed that at lower temperature i.e. 500 ^{o}C, the peaks were broader with low intensities indicating amorphous nature of the particles. However, with the increase of temperature i.e. 800 ^{o}C, the peaks became sharper with high intensities compared to lower temperature indicating that intensity increases

with the increase of temperature. The broadening of the peaks at lower temperature can also be attributed to the small particle size and sharper peaks with high intensities at higher temperature can be designated to the large particle size of the nanoparticles as reported in literature. This increase of intensity with the increase of temperature has also been reported by number of researchers [60 - 67]. Very recently, Amani-Beni and Nezamzadeh-Ejhieh, [65] presented XRD data for NiO and they claimed that the intensity of the peaks were increased by increasing the calcination temperature confirming the better crystallinity. They also claimed that peaks were broadened at lower temperature and thereafter narrower peaks were obtained, confirming the formation of smaller crystals at lower temperatures [62, 63, 68]. Senobari and Nezamzadeh-Ejhieh, [60] also recently reported that crystallinity of the photocatalyst (CuO-NiO) composite increases with the increase of temperature and hence aggregated particles are produced of which the peak width decreases with the increase of temperature [60, 65, 69]. These results indicate that peak intensity has direct relation with particle size. Mandal et al. [70] presented XRD patterns of different particle sizes of $NiFe_2O_4$ spinel ferrites nanoparticles and they observed that peaks became sharper with the increase in particle size [71, 72]. In XRD, the crystal planes at 110 and 200 correspond to the 2θ values of 44.81^o and 65.29^o belong to body centered cubic (BCC) phase of the Fe-Co alloy nanoparticles. The same phase behavior has been observed by many researchers [3, 13, 73-75]. Gurmen et al. [3] observed two main peaks of BCC crystalline phase of Co-Fe at the diffraction angles of 45^o and 65^o. Kodama et al. [75] synthesized Fe-Co nanoparticles using different metal ion concentrations and they observed the same BCC crystalline phase of Co-Fe alloy. However, they reported that the peak width at low concentration was comparatively broader than high concentration. In other words, bigger particles are formed at higher metal ion concentration. Wang et al. [73] also observed BCC crystalline phase however, they also observed face centered cubic (FCC) phase along with BCC phase. They also claimed that crystalline nanoparticle phases are dependent on Co contents in

Fe-Co alloy. They examined that the alloy contains less than 40wt% of Co, then have BCC structure and if the Co content exceeds 40wt%, the reflection of FCC can be distinguished. Wu et al. [76] fabricated the carbon encapsulated Fe-Co alloy nanoparticle using melamine as a carbon precursor. They also observed BCC structure, however they noted that the peak intensity of BCC Fe-Co decreases with increase of Co/Fe ratio. However, no sign of FCC phase structure is observed in our sample indicating that Co loading in our sample is less than 40wt%. EDS results in figure 6(c) also confirm that Co loading is less than 40% in Fe-Co alloy i.e. 35.83%.

In addition, at 800 ^{o}C, a very tiny peak at the 2θ value of 25.97^{o} is observed which may correspond to the crystal plane of carbon as shown in Fig 5. Sankar et al. [57] also observed the broad diffraction peak of carbon in the carbon coated $CoFe_2O_4$ at 2θ of 20 - 30^{o}. Wu et al. [73] reported the carbon peaks C (002) at the 2θ value of 25.97^{o} at different molar ratio of Fe-Co (1:1) to the carbon nanotubes and they noticed that relative intensity ratio of Fe-Co (110) peak to C (002) peak is increased with the increase of Fe-Co to carbon molar ratio. This peak at 800 ^{o}C may be appeared due to the reduction of CO_2 on Fe-Co ferrite nanoparticles. However, there was no obvious peak noticed at 500 ^{o}C. As CO disproportionation is more favorable at higher temperature as a result a carbon peak is observed at higher temperature rather than lower temperature. Tamaura and Tahata, [77] reported the complete reduction of CO_2 to C at 290 ^{o}C using bivalent metal oxides (ferrites) such as Fe, Ni, Co, Cu, Zn, Mg, and Mn etc. However, they used oxygen deficient ferrites represented by the general formula $M_xFe_{3-x}O_{4-\delta}$. The following reaction (1) for the CO_2 reduction on ferrite may occur as proposed by Tamaura and Tahata, [77].

$$M_xFe_{3-x}O_{4-\delta} + {}^{\delta}/_{2}\, CO_2 \rightarrow M_xFe_{3-x}O_4 + {}^{\delta}/_{2}\, C_{(s)} \qquad (1)$$

where M is the bivalent metal as mentioned above and δ is the reduction degree of ferrite.

In above reaction (1), O_2 in the CO_2 is transferred in the form of O^{2-} to the oxygen deficient $M_xFe_{3-x}O_{4-\delta}$. The C in the CO_2 is reduced to C by the addition of an electron donated from $M_xFe_{3-x}O_{4-\delta}$ so as to maintain electrical neutrality during the transfer of O^{2-} to $M_xFe_{3-x}O_{4-\delta}$.[77, 57]. Zheng et al. [78] reported the reduction of $scCO_2$ as a carbon source and the alkali metals (Na, Li) as the reductants to synthesize CNTs under reaction temperature of 600 – 750 ^oC. Hwang and Wang, [79] found that CO_2 reduction is mainly dependent on the compositions of the metal oxides and they claimed that Mn-Zn ferrites were much better than Mn-Ni ferrites. Lou et al. [80] used CO_2 as a carbon precursor for the synthesis of carbon nano materials (nano tubes) at the temperature and pressure values more than the supercritical state of CO_2 (critical point, 31 ^oC, 73 atm). In addition to it, they used longer reaction time about 10 hrs and they were able to synthesize carbon nano-tubes in an autoclave. However, they used Li as the reductant and the main products produced were carbon and Li_2CO_3 after reaction at 550 ^oC for 10 hrs. Xu and Huang, [81] successfully used CO_2 as carbon source for the synthesis of carbon nanotubes by CVD over Fe/CaO catalyst at a ratio of 1:10 using 45 minutes of reaction time at the temperature range from 790 to 810°C. They observed that nano tubes were formed at the temperature above 790 ^oC. Further increase in temperature, led to a branching structure of nano materials (main product) and at temperature above than 810 ^oC, no nano tubes were produced. In CVD process, the growth mechanism for the production of nano materials is generally related to the dissociation of carbon precursors in to carbon atoms, dissolution and saturation of these atoms in the catalyst metal particles and further precipitation into tubular carbon deposits as suggested by Xu and Huang, [81]. In the present process, nano-particles were successfully produced with smaller dimension at a relatively low temperature of 450°C and bigger dimension particles at high temperature of 800 ^oC, as the catalysts were packed loosely for efficient contact with the CO_2. However, during this process nanotubes were not formed which might indicate that cobalt oxide was acted as a support. As reported by Xu and Huang,

[81] that carbon nano tubes were not formed when normal catalysts supports such as MgO, SiO_2 and Al_2O_3 etc. were used. They also suggested that catalyst support is an important factor in the process of CO_2 decomposition and it will enhance absorption of CO_2 on the catalyst surface. So for the synthesis of nano particle, cobalt would enhance the absorption of CO_2 and would accelerate the decomposition of CO_2. On the other hand, the role of iron would be to catalyze the nanoparticle growth in the reaction process. Based on the data the typical characteristic peaks at 2θ values of 25.97°, 44.81° and 65.29° in XRD data of the sample shown in figure 5 have good agreement with the literature as well.

The EDS results presented in Fig. 6 also indicate the formation of carbon on all metal oxide samples used. The presence of carbon peaks indicates the effective CO disproportionation reaction because of which carbon peaks are appeared. The percent of carbon presence seems to be less in case of cobalt (1.22 wt%, figure 6a) than iron (1.94 wt%) and Fe-Co catalysts (4.52 wt%) as shown in the figures 6b and 6c, respectively. EDS analysis also indicate that mole ratio percents of C with respect to each metal is higher in Fe-Co catalyst than iron and cobalt catalysts. Mole ratio percents of C/Co, C/Fe and C/Co-Fe catalysts were found to be 7.4%, 13.67% and 27.36%, respectively. In addition, no impurity observed in the chemical composition shown in the tables embedded in the figure 6 (a,b,c) of the particles caused by other reaction products. However, it was observed that the weight percent of cobalt and iron are not same for Fe-Co catalyst i.e. weight percent of Fe is higher than Co. HRTEM analysis was also performed for cobalt, iron and Fe-Co catalysts at 600 °C as shown in figure 7 (a, b, c). This temperature is selected because of the CO disproportionation reaction which is kinetically and thermodynamically limited from 520 °C to 800 °C (Fig. 8). The resolution of the HRTEM image is not up to the mark indicating that the materials under study are magnetic i.e. particles are carbon coated [10]. The size of the particles are almost same as that found by the FESEM analysis. The average size of Co-Fe catalyst is found to be c.a. 55 nm. From the

HRTEM images of Co-Fe catalyst, thin layer is encapsulated over the surface of catalyst having thickness of about 2-3 nm. This layer is most probably carbon deposition [10] which is formed due to CO disproportionation reaction. El-Gendy et al. [10] found the Fe and Co spherical nanoparticles encapsulated with C. They observed the thickness of the carbon layer encapsulating the core particles amounts to 3–7 nm. In the case of Co, the carbon shells are rather similar to Fe but the core size distribution is slightly different. However, for the synthesis of the carbon coated Fe and Co nanoparticles, they used ferrocene and cobaltocene as precursors, respectively by using high pressure CVD process.

3.1.4. CO disproportionation process and its thermodynamic study (equilibrium constant and mole fraction relation)

Carbon dioxide reduction reactions for the CVD technique in which either a classical catalyst with supports or a floating catalyst is used as follows in reaction (2) as suggested by Simate et al. [59]:

$$2CO_2\,(g) \rightarrow 2CO\,(g) + O_2\,(g) \qquad (2)$$

The produced carbon monoxide has a simple disproportionation reaction as given below in equation 3, making it an ideal precursor for nano material synthesis:

$$2CO\,(g) \rightarrow C\,(s) + CO_2\,(g) \qquad (3)$$

This later reaction is an exothermic reaction as that of negative heat of reaction (ΔH = -171 kJ/mol) and hence it proceeds toward the initial product at high temperatures.

Thermodynamic study on the disproportionation reaction of CO for the Gibbs free energy with temperature is shown in figure 8. This data lead to the thermodynamic equilibrium constant relation as given below:

$$K = exp\left(\frac{175.76*T-171410}{R*T}\right) \qquad (4)$$

where, T is in K for a range of temperature from 350 ^{o}C to 1000 ^{o}C and R is the universal gas constant and its value is 8.314 J/mol.K. The intercept value (-171410) in the equation (4) is given as heat of reaction in J/mol. The temperature dependence of equilibrium mole fractions of CO and CO_2 at atmospheric pressure over the Fe-Co catalyst is also shown in figure 8. For the CO disproportionation reaction, delta G was found to be negative at all low temperatures (up to about 700 ^{o}C) and positive at all high temperature values. Gibbs energy was calculated from the following relation (equation 5) as given by Simth et al. [82]:

$$\frac{\Delta G^{o}}{RT} = \frac{\Delta G_0^{o} - \Delta H_0^{o}}{RT_0} + \frac{\Delta H_0^{o}}{RT} + \frac{1}{T}\int_{T_0}^{T} \frac{\Delta C_P^{o}}{R} dT - \int_{T_0}^{T} \frac{\Delta C_P^{o}}{R} \frac{dT}{T} \qquad (5)$$

Where ΔG_0^{o} and ΔH_0^{o} are Gibbs energy and enthalpy of formations at standard state and 298.15 K temperature, ΔC_P^{o} and ΔG^{o} are the specific heat capacity and Gibbs energy at standard state and T_0 is the reference temperature i.e. 298.15 K. Values of the Cp constants i.e. A, B, C and D and standard state Gibbs energy and enthalpy of formations at 298.15 K are taken from Smith et al. [82] as shown in table 2. Other thermodynamic property such as entropy change at standard state (ΔS_0^{o}) was calculated by using the following equation (6) [82].

$$\Delta G_0^{o} = \Delta H_0^{o} - T\Delta S_0^{o} \qquad (6)$$

Based on the equation (4), the equilibrium constant values were found to be decreased with the increase of temperature (at all temperature ranges) as expected. However relation found not to be linear. At lower temperatures, it decreases sharply upto about 650 ^{o}C and afterwards it decreases slowly because of the change in Gibbs energy from negative to positive. The temperature dependence of equilibrium mole fractions of CO and CO_2 at atmospheric pressure over the Fe-Co catalyst were also calculated by assuming CO disproportionation reaction as a gaseous reaction. In addition, the activity of the graphite carbon (a_C) was also assumed to be 1. The equilibrium constant in terms of activities i.e. equation (7) comes out to be as follows:

$$K = \frac{a_C\, a_{CO_2}}{a_{CO}{}^{2}} = \frac{p_{CO_2}}{p_{CO}} \qquad (7)$$

Writing above equation (7) in terms of mole fraction as follows:

$$K = \frac{y_{CO_2}}{(y_{CO})^2 \times P} = \frac{y_{CO_2,0} + X_A\, y_{CO,0}}{\left(y_{CO,0} - 2X_A\, y_{CO,0}\right)^2 \times P} \qquad (8)$$

where a, y, p and P are the activity, mole fraction, partial pressure and total pressure, respectively. Mole fractions of y_{CO} and y_{CO_2} were obtained by equating equation (8) and equation (4) at respective temperature using solver in excel. It is observed that the kinetic and thermodynamic factors limit this particular reaction in the particular temperature range at atmospheric pressure as observed by Moisala et al. [83]. However, this range is undesirable for the dissolution of carbon and the subsequent precipitation step on the metal particles. Moisala et al. [83] observed the kinetic and thermodynamic factors limitation for the effective CO disproportionation reaction and found out that it happened for a temperature range of 520 – 800 ^{o}C at normal pressure. However, they claimed that this temperature range may not be optimal for carbon dissolution and precipitation from the metal particle.

Conclusions

Carbon coated nano-particles exhibiting pebble-like shapes, with some of conjoined shapes, or nano-beads were successfully produced under CO_2 environment using CCVD process in TGA. The reaction temperature was found to be an important parameter in determining the nature (amorphous or crystalline), and controlling the growth (size and shape) of the nano-particles. In FESEM, on Fe, Co and Fe-Co catalysts, increasing temperature will lead to greater particle size, sphericity and crystallinity. On the other hand, at low temperature, particles were found to be small and amorphous in nature. Among all produced nanoparticles (Fe, Co, Fe-Co), the size of Fe nanoparticles were found to be the smallest at all temperatures. Compared to FESEM, XRD shows similar results as that of FESEM. In XRD, it was observed that at lower temperature i.e. 500 ^{o}C, the peaks were broader with low intensities indicating amorphous nature and small particle size of the particles. However, with the increase of

temperature i.e. 800 ^{o}C, the peaks became sharper with high intensities compared to lower temperature indicating crystalline nature and larger particle size of the nanoparticles. It also reflects that intensity increases with the increase of temperature. The crystal planes observed were belong to BCC phase of the Fe-Co nanoparticles, however, no FCC phase was observed. This indicates the dominant effect of Fe on Co in Fe-Co ferrite catalyst. In addition, the size of the Fe-Co nano-particles is close to Fe which also reflects dominancy of Fe in Fe-Co catalysts. This dominant effect of Fe may be due to high weight percent of Fe than Co in the sample as noticed in EDS analysis. A very tiny peak of carbon at 2 theta value of 25.97^{o} was also observed at 800 ^{o}C which may be appeared due to the reduction of CO_2 on Fe-Co ferrite nanoparticles. However, no obvious peak could be noticed at 500 ^{o}C indicating that CO disproportionation reaction is more favorable at higher temperature. Carbon deposition was also observed on Fe-Co ferrite at 600 ^{o}C by HRTEM and EDS analyses. In EDS, the percent of carbon presence seems to be highest in case of Fe-Co ferrite (4.52 wt%) than iron (1.94 wt%) and cobalt (1.22 wt%). Using TEM, particle sizes of the Fe, Co and Fe-Co ferrite nanoparticles were found to be approximately same as that of FESEM. In addition, carbon thin layer of thickness *c.a.* 2-3 nm was also noticed in HRTEM image of Co-Fe catalyst. Equations for equilibrium constant, Gibbs free energy and mole fractions (y_{CO} and y_{CO_2}) were developed and CO disproportionation reaction for carbon deposition was studied for a wide temperature range. The equilibrium constant values were found to be decreased with the increase of temperature. However, Gibbs free energy were observed to be changed from negative to positive with the increase of temperature. It was noticed that CO decomposition is thermodynamically limited from 520 to 800 ^{o}C which led to carbon deposition on the catalyst as observed by the carbon presence in EDS, XRD and HRTEM images i.e. the encapsulation of thin layer of carbon on the Fe-Co particles.

References

[1] Z.H. Wang, C.J. Choi, B.K. Kim, J.C. Kim, Z.D. Zhang, J. Alloys Comp. 351 (2003) 319-323.

[2] B. Zhou, S. Hermans, S. Somorjai, Nanotechnology in Catalysis, Kluwer Academic/Plenum Publishers, New York, 2004.

[3] S. Gurmen, A. Guven, B. Ebin, S. Stopic, B. Friedrich, J. Alloys Comp. 481 (2009) 600-604.

[4] V. Jokanovic, Struct. Substruct. Spray Pyrol. Proc.: Nanodesign., Surfact. Sci. Ser., 130 (2006) 513-533.

[5] R.W. Siegel, Nanophase Materials: Synthesis, Structure, and Properties, Springer, Verlag, 1994.

[6] H. Derikvandi, A. Nezamzadeh-Ejhieh, J. Molecular Catal. A: Chem. 426 (2017) 158–169.

[7] S. Sharafzadeh, A. Nezamzadeh-Ejhieh, Electrochim. Acta 184 (2015) 371–380.

[8] D. Yang, X. Ni, D. Zhang, H. Zheng, J. Cheng, P. Li, J. Cryst. Growth. 286 (2006) 152-155.

[9] Y.G. Chin, H.J. Wernich, E.P. Wohlfarth, Ferromagn. Mat. North-Holland, Amsterdam, 1980.

[10] A.A. El-Gendy, E.M.M. Ibrahim, V.O. Khavrus, Y. Krupskaya, S. Hampel, A. Leonhardt, B. Buchner, R. Klingeler, 'Carbon'. 47 (2009) 2821-2828.

[11] A. Yadav, R. Kumar, H.K. Choudhary, B. Sahoo, 'Carbon'. 140 (2018) 477 – 487.

[12] N. Luo, X. Li, X. Wang, H. Yan, C. Zhang, H. Wang, 'Carbon'. 48 (2010) 3858-3863.

[13] B.H. Lee, Y.J. Lee, K.H. Min, D.G. Kim, Y.D. Kim, Mat. Lett. 59 (2005) 3156-3159.

[14] M. D.Y. Alicia, Y. Oumellal, C. Zlotea, L. Vidal, M. G. Camelia, Nano-Struct. Nano-Objects 9 (2017) 1– 12.

[15] G. Nam, J. Park, M. Choi, P. Oh, S. Park, M.G. Kim, N. Park, J. Cho, J-S. Lee, ACS Nano. 9 (2015) 6493–6501.

[16] X. Xu, J. Liu, J. Liu, L. Ouyang, R. Hu, H. Wang, L. Yang, M. Zhu, Adv. Funct. Mater. 28 (2018) 1–12.

[17] S. Suriyakumar, N. Angulakshmi, A. M. Stephan, Nano-Struct. Nano-Objects 11 (2017) 46–55.

[18] M. Liu, M. Shi, W. Lu, D. Zhu, L. Li, L. Gan, Chem. Eng. J. 313 (2017) 518–526.

[19] A. Meffre, B. Mehdaoui, V. Kelsen, P.F. Fazzini, J. Carrey, S. Lachaize, M. Respaud, B. Chaudret, Nano Lett. 12 (2012) 4722–4728.

[20] D. Lin, T. Qin, Y. Wang, X. Sun, L. Chen, ACS Appl. Mater. Interfaces, 6 (2014) 1320–1329.

[21] D. Vilela, J. Parmar, Y. Zeng, Y. Zhao, S. Sánchez, Nano Lett. 16 (2016) 2860–2866.

[22] P. Trogadas, T.F. Fuller, P. Strasser, 'Carbon'. 75 (2014) 5 – 42.

[23] R. Kumar, H.K. Choudhary, S.P. Pawar, S. Bose, B. Sahoo, Phys. Chem. Chem. Phys. 19 (2017) 23268–23279.

[24] Y. Wang, H. Sun, X. Duan, H.M. Ang, M.O. Tadé, S. Wang, Appl. Catal. B Environ. 172–173 (2015) 73–81.

[25] Y. Ai, L. Liu, K. Jing, L. Qi, Z. Fan, J. Zhou, H. Sun, Z. Shao, Q. Liang, Nano-Struct. Nano-Objects 10 (2017) 116–124.

[26] A. Naghash, A. Nezamzadeh-Ejhieh, J. Ind. Eng. Chem. 31 (2015) 185–191.

[27] S. Dürr, C. Janko, S. Lyer, P. Tripal, M. Schwarz, J. Zaloga, R. Tietze, C. Alexiou, Nanotechnol. Rev. 2 (2013) 395–409.

[28] F.F. Fang, H.J. Choi, Colloid Polym. Sci. 288 (2010) 79–84.

[29] C.E. Cava, R. Possagno, M.C. Schnitzler, P.C. Roman, M.M. Oliveira, C.M. Lepiensky, A.J.G. Zarbin, L.S. Roman, Chem. Phys. Lett. 444 (2007) 304– 308.

[30] J. Szczytko, P. Osewski, M. Bystrzejewski, J. Borysiuk, A. Grabias, A. Huczko, H. Lange, A. Majhofer, A. Twardowski, Acta Phys. Polon. A. 112 (2007) 305–310.

[31] J. Orozco, L. A. Mercante, R. Pol, A. Merkoçi, J. Mater. Chem. A 4 (9) (2016) 3371–3378.

[32] H. Niu, Y. Wang, X. Zhang, Z. Meng, Y. Cai, ACS Appl. Mater. Interfaces 4 (2012) 286–295.

[33] K.B. Tan, M. Vakili, B.A. Horri, P.E. Poh, A.Z. Abdullah, B. Salamatinia, Sep. Purif. Technol. 150 (2015) 229–242.

[34] M. Bystrzejewski, O. Łabędź, W. Kaszuwara, a. Huczko, H. Lange, Powder Technol. 246 (2013) 7–15.

[35] B. David, O. Schneeweiss, N. Pizurova, M. Klementová, P. Bezdička, R. Alexandrescu, F. Dumitrache, I. Morjan, Surf. Interface Anal. 38 (2006) 482–485.

[36] E.T. Thostenson, Z. Ren, T.W. Chou, Comp. Sci. Tech. 61 (2001) 1899-1912.

[37] D. Ding, Z-L. Song, Z-Q. Cheng, W-N. Liu, X-K. Nie, X. Bian, Z. Chen, W. Tan, J. Mater. Chem. A, 2 (2014) 472–477.

[38] R. Kumar, B. Sahoo, Nano-Structures & Nano-Objects 16 (2018) 77–85.

[39] A. Soni, L. Zhao, H. Q. Ta, Q. Shi, J. Pang, P. S. Wrobel, T. Gemming, A. Bachmatiuk, M. H. Rummeli, Nano-Structures & Nano-Objects 16 (2018) 38–44.

[40] N. Luo, K-X. Liu, Z-Y. Liu, X-J. Li, S-Y. Chen, Y. Shen, T-W. Chen, Nanotechnology 23 (2012) 475603.

[41] N.Y. He, Y.F. Guo, Y. Deng, Z.F. Wang, S. Li, H.N. Liu, Chin. Chem. Lett. 18 (2007) 487–490.

[42] R. Kumar, R. Rajendiran, H.K. Choudhary, G.M. Naveen Kumar, B. Balaiah, A.V. Anupama, B. Sahoo, Nano-Struct. Nano-Objects 12 (2017) 229–238.

[43] S. Yallappa, D.R. Deepthi, S. Yashaswini, R. Hamsanandini, M. Chandraprasad, S. Ashok Kumar, G. Hedge, NanoStruct. Nano-Objects 12 (2017) 84 – 90.

[44] R. Kumar, B. Sahoo, NanoStruct. Nano-Objects. 14 (2018) 131–137.

[45] R. Sergiienko, E. Shibata, S. Kim, T. Kinota, T. Nakamura, 'Carbon'. 47 (2009) 1056–1065.

[46] T.C. Schmitt, A.S. Biris, D.W. Miller, A.R. Biris, D. Lupu, S. Trigwell, Z.U. Rahman, 'Carbon'. 44 (2006) 2032-2038.

[47] H. Kathyayini, I. Willems, A. Fonseca, J.B. Nagy, N. Nagaraju, Catal. Comm. 7 (2006) 140-147.

[48] D. Anne-Claire, Prog. Mat. Sci. 50 (2005) 929-961.

[49] V. M. Sivakumar, A.Z. Abdullah, A.R. Mohamed, S.P. Chai, J. Nanomat. Biostruc. 5 (2010) 691 – 698.

[50] J. Wen, W. Chu, C. Jiang, D. Tong, J. Nat. Gas Chem. 19 (2010) 156-160.

[51] I. Shao P.M. Vereecken, C.L. Chien, R.C. Cammarata, P.C. Searson, J. Electrochem. Soc. 150 (2003) C184 – C188.

[52] D. Kim, D.Y. Park, B.Y. Yoo, P.T.A. Sumodjo, N.V. Myung, Electrochim Acta. 48 (2003) 819 - 830.

[53] D. Gautard, G. Couderchon, L. Coutu, J. Magn. Magn. Mater. 160 (1996) 359 - 360.

[54] C. H. Shang, T. P. Weihs, R.C. Cammarata, Y. Ji, C.L. Chien, J. Appl. Phys. 87 (2000) 6508 - 6510.

[55] M.F. Irfan, M.H. Chakrabarti, K. Kusakabe, Can. J. Chem. Eng. 91 (2013) 1936 – 1944.

[56] T. Ch, L. Ch, A. Gloter, V. Serin, G. Nihoul, Int. J. Inorg. Mater. 3 (2001) 1025-1031.

[57] K.V. Sankar, S. Shanmugapriya, S. Surendran, S. C. Jun, R. K. Selvan, J. Coll. Interf. Sci. 513 (2018) 480 – 488.

[58] L. Ajroudi, N. Mliki, L. Bessais, V. Madigou, S. Villain, Ch. Leroux, Mat. Res. Bullet. 59 (2014) 49–58.

[59] G.S. Simate, S.E. Iyuke, S. Ndlovu, C.S. Yah, L.F. Walubita, J. Nat. Gas Chem. 19 (2010) 453-460.

[60] S. Senobari, A. Nezamzadeh-Ejhieh, J. Mol. Liq. 261 (2018) 208–217.

[61] Y. Qu, H. Yang, N. Yang, Y. Fan, H. Zhu, G. Zou, Mat. Lett. 60 (2006) 3548–3552.

[62] H. Derikvandi, A. Nezamzadeh-Ejhieh, J. Col. Interf. Sci. 490 (2017) 314–327.

[63] H. Derikvandi, A. Nezamzadeh-Ejhieh, J. Hazard. Mater. 321 (2017) 629–638.

[64] S. Senobari, A. Nezamzadeh-Ejhieh, J. Mol. Liq. 257 (2018) 173–183.

[65] Z. Amani-Beni, A. Nezamzadeh-Ejhieh, Anal. Chim. Acta. 1031 (2018) 47–59.

[66] M.M. El-Okr, M.A.Salem, M.S.Salim, R.M.El-Okr, M.Ashoush, H.M.Talaat, J. Magnet. Magnet. Mat. 323 (2011) 920–926.

[67] M. F. Irfan, J. H. Goo, S. D. Kim, Appl. Catal. B: Environ. 78 (2008) 267–274.

[70] K. Mandal, S. Mitra, P. A. Kumar, Europhys. Lett.,75 (2006) 618–623.

[71] I. V. Beketov, A. P. Safronov, A. I. Medvedev, J. Alonso, G. V. Kurlyandskaya, S. M. Bhagat, AIP Advances 2 (2012) 022154 (1- 24).

[72] J. H. Grossman, S. E. McNeil, Physics Today, 65 (2012) 38 - 42.

[73] Z.H. Wang, C.J. Choi, J.C. Kim, B.K. Kim, Z.D. Zhang, Mat. Lett. 57 (2003) 3560–3564.

[74] H-Q. Wu, P-S. Yuan, H-Y. Xu, D-M. Xu, B-Y. Geng, X-W. Wei, J. Mat. Sci. 41 (2006) 6889–6894.

[75] D. Kodama, K. Shinoda, K. Sato, Y. Sato, B. Jeyadevan, K. Tohji, J. Magnet. Magnet. Mat. 310 (2007) 2396–2398.

[76] A. Wu, X. Yang, H. Yang, Dalton Trans. 42 (2013) 4978 – 4984.

[77] Y. Tamaura, M. Tahata, Nature. 346 (1990) 255 - 256.

[78] L.Y. Zheng, L.X. Zhao, Y.Z. Wan, Y.L. Wang, W.H. Xiong, ‘Carbon’. 43 (2005) 1084 - 1089.

[79] C.S. Huwang, N.C. Wang, Mater. Chem. Phys. 88 (2004) 258 - 263.

[80] Z.S. Lou, Q.W. Chen, W. Wang, Y.F. Zhang, ‘Carbon’. 41 (2003) 3063 - 3067.

[81] X.J. Xu, S.M. Huang, Mater. Lett. 61 (2007) 4235 - 4237.

[82] J.M. Smith, H.C. Van Ness, M.M. Abbott, Introduction to Chemical Engineering Thermodynamics, 7th edition, McGraw Hill, 2005.

[83] A. Moisala, A.G. Nasibulin, E.I. Kauppinen, J. Phys: Condens. Matter. 15 (2003) S3011 – S3035.

Acknowledgement

The authors would like to thank the Nanocen at University of Malaya, Malaysia and Nanotechnology Center / Central Labs at College of Science, University of Bahrain, Kingdom of Bahrain for allowing to use the analytical equipment.

Figure captions

Figure 1. TG-DTG curves for the production of nano-particles over Fe-Co catalyst at reaction temperature of 500°C

Figure 2. FESEM images (20 kx & 80 kx) of the carbon-encapsulated cobalt nano-particles synthesized under CO_2 environment at (a) 450 °C (b) 500 °C (c) 600 °C (d) 650 °C

Figure 3. FESEM images (20 kx & 80 kx) of the carbon-encapsulated iron nano-particles synthesized under CO_2 environment at (a) 450 °C (b) 500 °C (c) 600 °C (d) 650 °C

Figure 4. FESEM images (20 kx & 80 kx) of the carbon-encapsulated Fe-Co nano-particles synthesized under CO_2 environment at (a) 450 °C (b) 500 °C (c) 600 °C (d) 700 °C (e) 750 °C (f) 800 °C (g) 1000 °C

Figure 5. XRD patterns of carbon encapsulated Fe-Co alloy nanoparticles at 500 and 800 ^oC temperatures

Figure 6. EDS patterns of carbon-encapsulated (a) cobalt (b) iron and (c) Fe-Co nano-particles.

Figure 7. TEM images of carbon encapsulated (a) cobalt, (b) iron and (c) Fe-Co nano-particles at 600 ^oC

Figure 8. Equilibrium concentration of CO disproportionation reaction for the carbon deposition along with Gibbs energy and equilibrium constant

List of Tables

Table 1. Summary of the mass changes of the catalysts

Table 2. All Cp constants, Gibbs energy and Enthalpy of formations at standard state and 298.15 K.

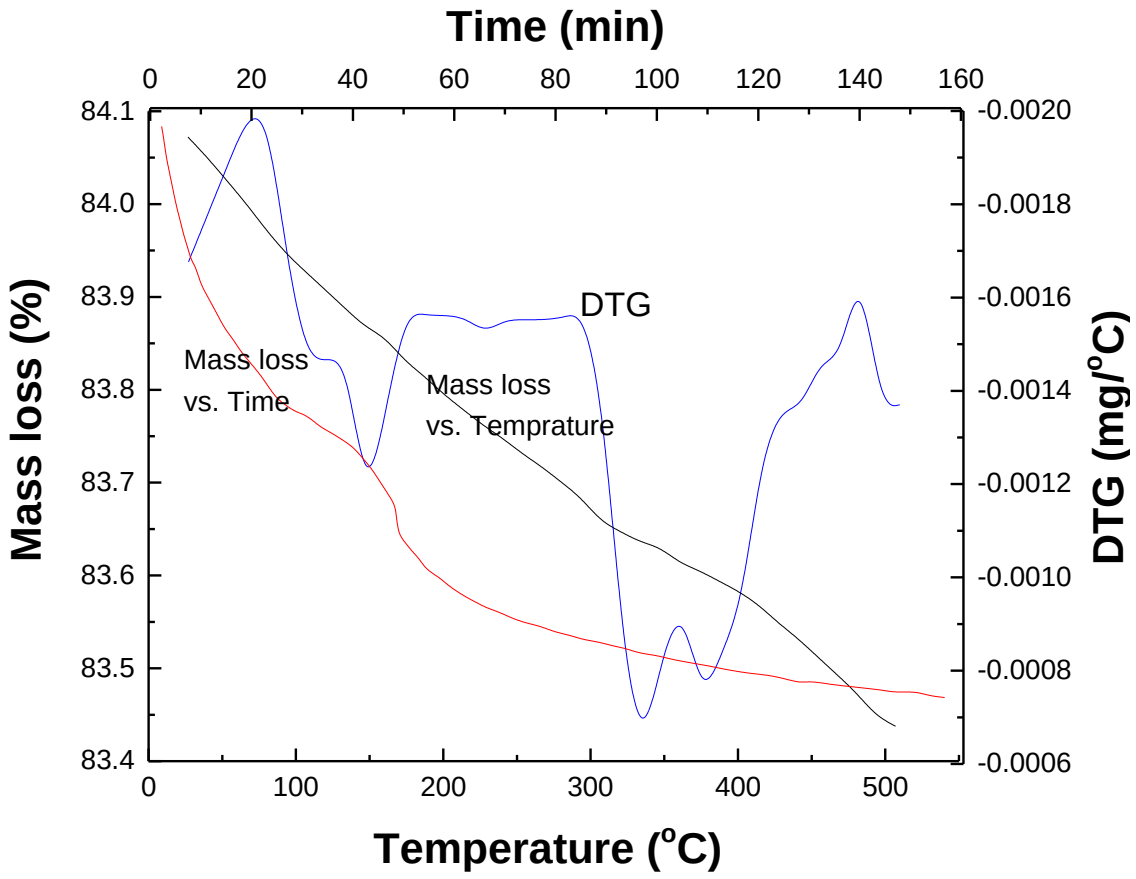
Time (min)
0
20
40
60
80
100
120
140
160
84.1
84.0
83.9
83.8
83.7
83.6
83.5
83.4
-0.0020
-0.0018
-0.0016
-0.0014
-0.0012
-0.0010
-0.0008
-0.0006
Mass loss (%)
DTG (mg/°C)
DTG
Mass loss
vs. Time
Mass loss
vs. Temprature
0
100
200
300
400
500
Temperature (°C)

Figure 1

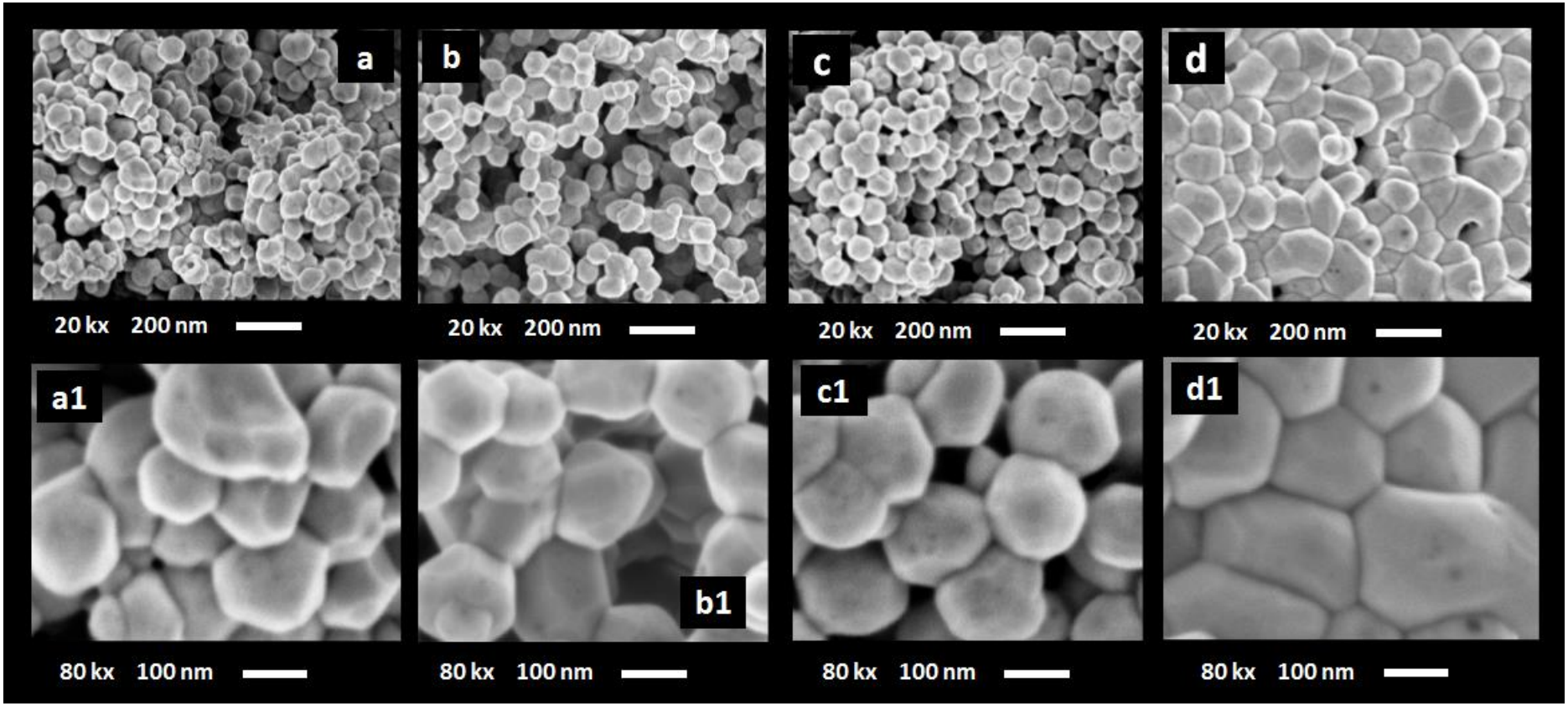
a
b
c
d
20 kx 200 nm
20 kx 200 nm
20 kx 200 nm
20 kx 200 nm
a1
b1
c1
d1
80 kx 100 nm
80 kx 100 nm
80 kx 100 nm
80 kx 100 nm

Figure 2

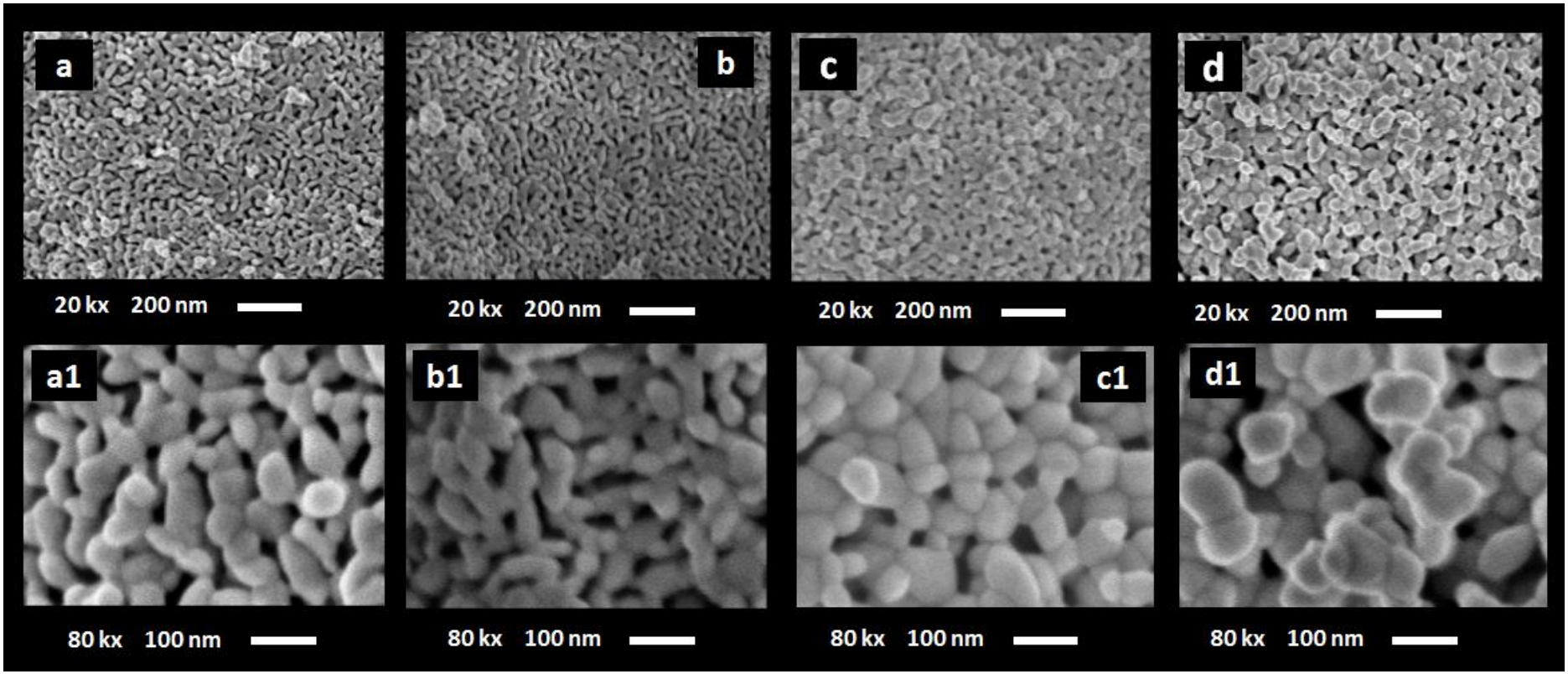
a
b
c
d
20 kx 200 nm
20 kx 200 nm
20 kx 200 nm
20 kx 200 nm
a1
b1
c1
d1
80 kx 100 nm
80 kx 100 nm
80 kx 100 nm
80 kx 100 nm

Figure 3

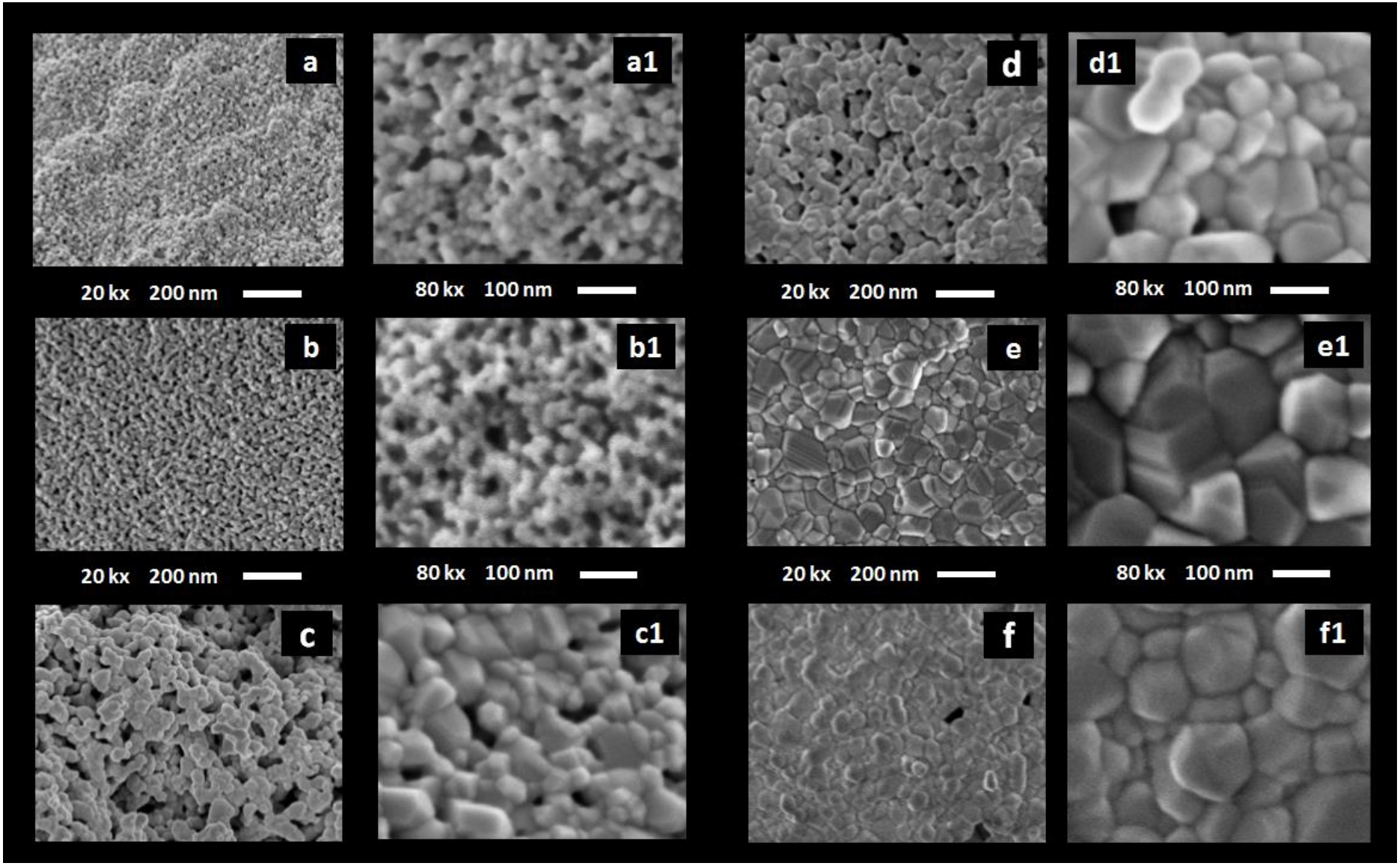
a
a1
d
d1
20 kx 200 nm
80 kx 100 nm
20 kx 200 nm
80 kx 100 nm
b
b1
e
e1
20 kx 200 nm
80 kx 100 nm
20 kx 200 nm
80 kx 100 nm
c
c1
f
f1

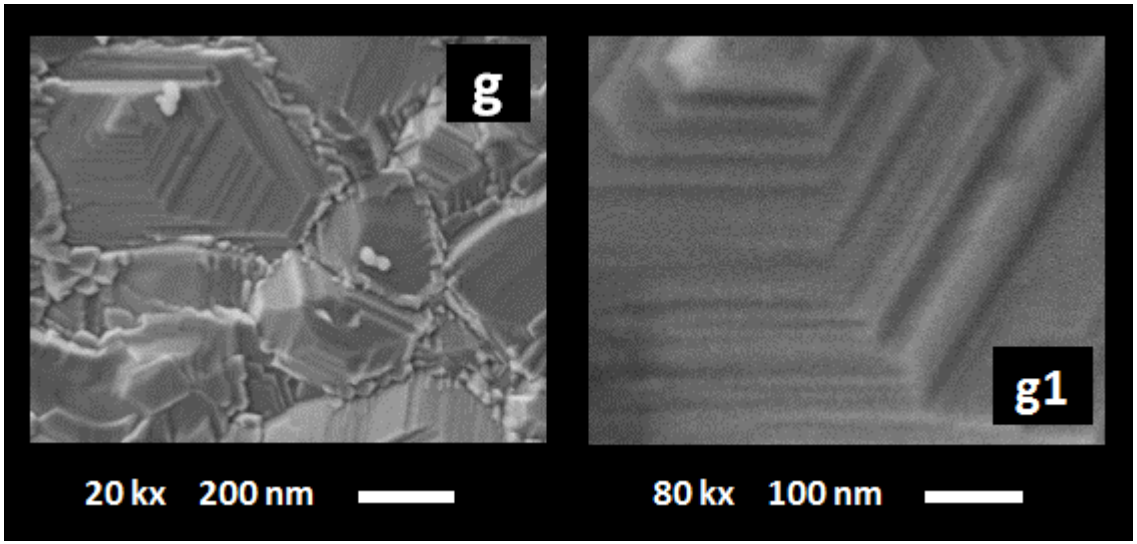

Figure 4

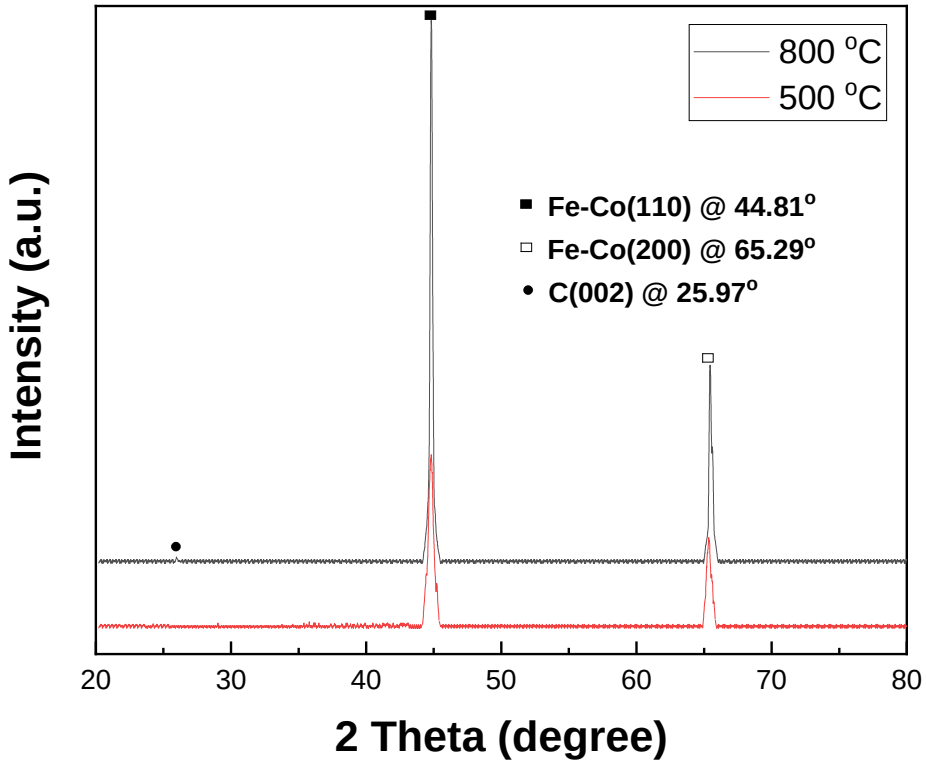
800 °C
500 °C
Fe-Co(110) @ 44.81°
Fe-Co(200) @ 65.29°
C(002) @ 25.97°
Intensity (a.u.)
20
30
40
50
60
70
80
2 Theta (degree)

Figure 5

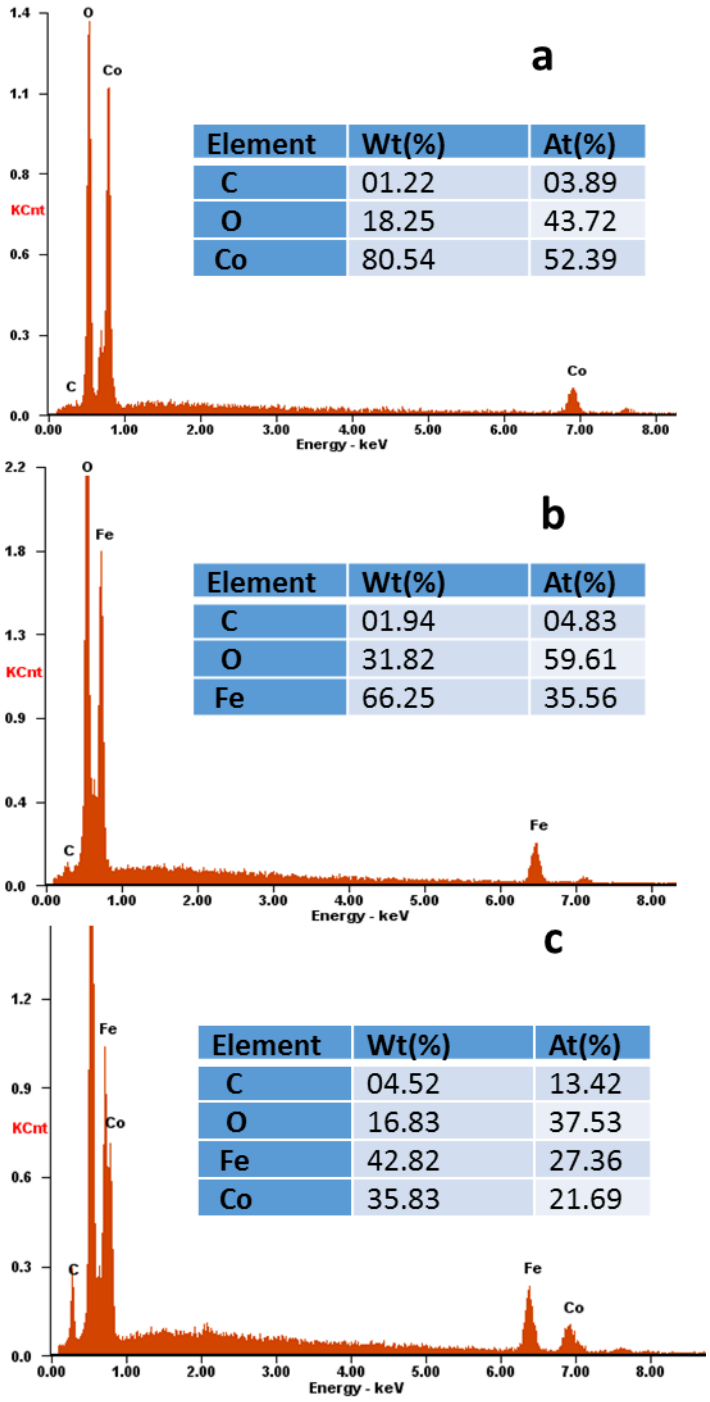
a
Element | Wt(%) | At(%)
C | 01.22 | 03.89
O | 18.25 | 43.72
Co | 80.54 | 52.39
O
Co
C
Co
KCnt
Energy - keV
b
Element | Wt(%) | At(%)
C | 01.94 | 04.83
O | 31.82 | 59.61
Fe | 66.25 | 35.56
O
Fe
C
Fe
KCnt
Energy - keV
c
Element | Wt(%) | At(%)
C | 04.52 | 13.42
O | 16.83 | 37.53
Fe | 42.82 | 27.36
Co | 35.83 | 21.69
Fe
Co
C
Fe
Co
KCnt
Energy - keV

Figure 6

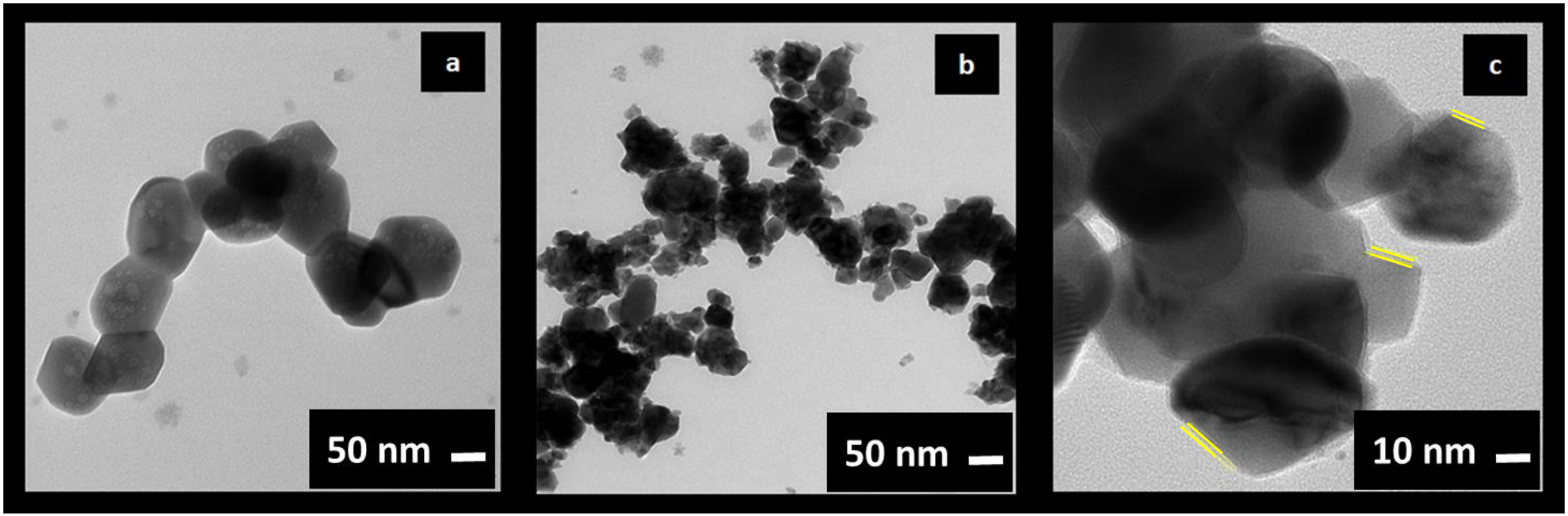

Figure 7

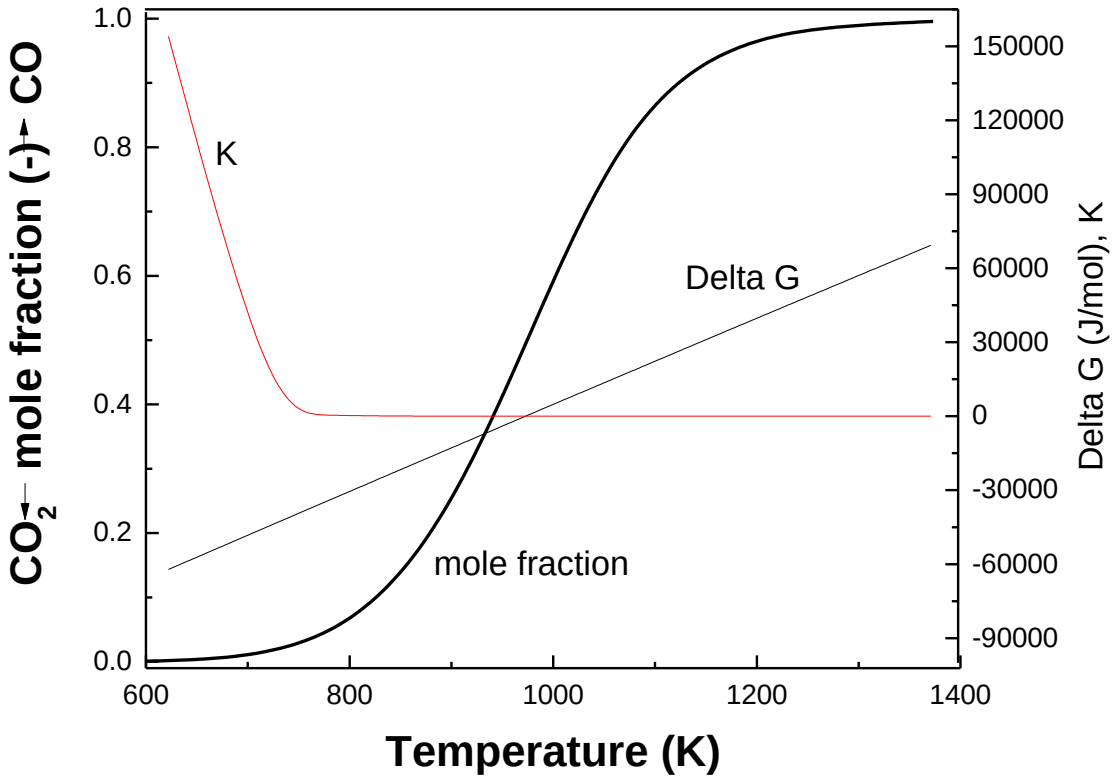
1.0
0.8
0.6
0.4
0.2
0.0
600
800
1000
1200
1400
150000
120000
90000
60000
30000
0
-30000
-60000
-90000
K
Delta G
mole fraction
Temperature (K)
Delta G (J/mol), K
CO2 mole fraction (-)→ CO

Figure 8

Table 1

Catalyst	Final Temperature (ºC)	Over all Mass Loss (mg)
Fe (Sample 1)	500	0.6530
Co (Sample 2)	500	0.6179
Fe-Co (Sample 3)	500	0.6450
Fe-Co (Sample 4)	450	0.3958
Fe-Co (Sample 5)	600	0.6979

Table 2

Components	ΔCp constants				ΔH_0^o (J/mol)	ΔG_0^o (J/mol)	ΔS_0^o (J/mol.K)
	A	B×10^3	C×10^6	D×10^{-5}			
CO	3.376	0.557	0	-0.031	-110525	-137169	89.364
CO_2	5.457	1.045	0	-1.157	-393509	-394359	2.851
C	1.771	0.771	0	-0.867	0	0	0